Graphene Logic Gates

Savvas Moysidis, Ioannis G. Karafyllidis, and Panagiotis Dimitrakis, *Senior Member, IEEE*

***Abstract*—Graphene is a biocompatible material that can be incorporated safely into living tissue. This property makes graphene an ideal material for bioelectronics applications. The main obstacle for using graphene as a material for bioelectronic circuits is the lack of a bandgap, which results in noneffective current switching. Here, we use rectangular L-shaped graphene nanoribbons as a building block for graphene logic gates. Electrons are initially transported along the zigzag-edged nanoribbon and then the transport direction changes by 90°, resulting in transport along the armchair edge. Our computations showed that electron scattering because of this change in the direction causes the appearance of a pseudobandgap, which is large enough for logic operations. This pseudobandgap appears as a zero-conductance region for electron energies near the Fermi level. We propose an AND, an OR, and a NOT logic gate and use tight-binding Hamiltonians and nonequilibrium Greens functions to show that these designs can reproduce effectively the desired logic operations.**

***Index Terms*—Nanoelectronic circuits, graphene, nanoribbon, nioelectronics.**

I. Introduction

CIRCUITS for bioelectronics are most effective when incorporated into living tissue providing a reliable interface with minimal invasiveness. These circuits are expected to operate reliably in a noisy environment and the circuit material should be chemically stable [1], [2]. One of the most challenging applications is in neural prosthetics, where these circuits are expected to monitor the low-voltage operation of neural cells, stimulate their activity and provide drug screening [3]. Graphene is a biocompatible material, which is remarkably stable in biological environments [4]. The high electrical conductance of graphene nanoribbons ensures high signal-to-noise rations in signal reception and transmission form neural cells to electronic circuits and vice versa [5]. Because of ballistic transport, graphene nanoribbons retain their high conductance when scaled down to very small sizes. This fact allows dense packaging of interconnections resulting in high resolution probes that can map with precision the electrical activity of neuron cells [3], [5]. High thermal conductivity combined with ballistic transport result in very low energy dissipation in graphene interconnects, which is vital for sensing and controlling the delicate activity of neural cells.

Furthermore, graphene nanoribbons are very reliable interconnects, because of their chemical stability, flexibility and very high tensile strength [6], and integration of graphene into tissue causes minimal disruption of tissue form and function [7]. There is also strong evidence that the high electrical and thermal conductivity of graphene promotes cell proliferation and reconstruction of tissue defects caused by infection, trauma and tumors, and, as a secondary function, because of its mechanical properties and stability, graphene can provide scaffolding to support traumatized tissue [8].

All the properties described above, make graphene nanoribbons reliable, stable and effective electrodes and interconnects between tissue and information processing electronic circuits. It would be very desirable if a part of the information processing circuit could be placed very close to the graphene electrodes and interconnects, but silicon-based circuit integration with tissue presents several problems some of which are unsurmountable [9], [10]. Graphene-based logic circuits can be easily connected to graphene electrodes and interconnects and can also be integrated with tissue, but graphene is a gapless material, and because of that, currents cannot be effectively switched off. It has been shown that graphene quantum point contacts and graphene p-n junctions can effectively switch off currents, but these devices require back gates which are fabricated by placing graphene nanoribbons on a relative thick (300 nm) substrate of SiO_2 [11], [12], forbidding their safe integration into tissue. Graphene logic circuits that do not require back gates will leave one of the sides of the two-dimensional graphene sheet unaltered and free to be placed on tissue, very close to graphene electrodes and interconnects.

In this work we design and simulate the operation of graphene logic gates that do not require back gating. We use L-shaped graphene nanoribbons and top gates to construct the logic gates. In section two, we compute the band structure of L-shaped graphene nanoribbons and show that the change of electron transport direction by 90°, i.e., from the zigzag edged to the armchair edged part of the L-shaped structure, gives rise to a pseudo-bandgap, large enough for logic operations. In section three we describe briefly the method we use to compute the conductance of graphene logic gates from input to output, namely the tight-binding Hamiltonians and the non-equilibrium Green's functions. In sections four, five and six we present the designs and the simulated operation of the AND, OR and NOT gates, respectively. In section seven we present our conclusions.

Manuscript received January 16, 2018; revised April 17, 2018; accepted May 31, 2018. Date of publication June 13, 2018; date of current version July 9, 2018. This work of S. Moysidis was supported in part by the General Secretariat for Research and Technology (GSRT) and in part by the Hellenic Foundation for Research and Innovation (HFRI). The review of this paper was arranged by Associate Editor Z. Zhong. *(Corresponding author: Ioannis G. Karafyllidis.)*

S. Moysidis and I. G. Karafyllidis are with the Department of Electrical and Computer Engineering, Democritus University of Thrace, Xanthi 67100, Greece (e-mail: smoysidi@ee.duth.gr; ykar@ee.duth.gr).

P. Dimitrakis is with the Institute of Nanoscience and Nanotechnology, NCSR "Demokritos," Athens 60037, Greece (e-mail: p.dimitrakis@inn.demokritos.gr).

Digital Object Identifier 10.1109/TNANO.2018.2846793

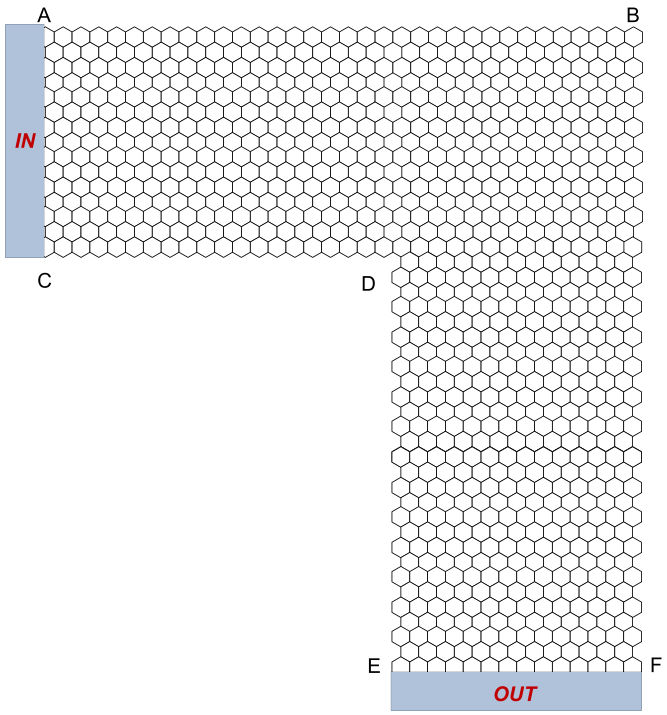

Fig. 1. L-shaped graphene nanoribbon. Electrons are transported from the input (IN) contact to the output (OUT) contact. Edges AB, and CD are zigzag, and edges BF and DE armchair.

II. L-Shaped Graphene Nanoribbons

An L-shaped graphene nanoribbon is shown in Fig. 1. Electrons enter the structure through the input contact, IN and are transported towards the output contact, OUT. The AB and CD edges of the L-shaped nanoribbon are zigzag edges, whereas the BF and DE are armchair edges.

The energy band structure of the entire L-shaped graphene nanoribbon cannot be computed analytically, because of the lack of symmetry in the transition region from the zigzag to the armchair edges. We computed the *E-k* relations in the zigzag and armchair parts of the structure, where the electrons enter and exit. For our computations we used a tight-binding Hamiltonian, *H*, which describes electron transport between nearest-neighbor carbon atoms [13], [14]:

$$H = \sum_{i,j} (-t_{i,j})\, \hat{c}_i^{\dagger}\, \hat{c}_j = \tau \sum_{i,j} \hat{c}_i^{\dagger}\, \hat{c}_j \qquad (1)$$

The index *j* indicates the atom where an electron is located during an infinitesimal time interval and the index *i* runs over the three nearest neighboring carbon atoms. The electron motion is described using fermion annihilation and creation operators. Electron motion is associated with a kinetic energy $t_{i,j}$ which is the overlap integral. The value of $t_{i,j}$ is the same for the three neighboring atoms and is symbolized by τ: $-t_{i,j} = \tau \cong -2.7$ eV [5], [6]. The overlap integral between non-neighboring carbon atoms is zero.

The computed *E-k* relations for the zigzag and armchair parts of the L-shaped graphene nanoribbon of Fig. 1 are shown in Fig. 2. Electrons that participate in conductance are a few *kT* below and above the Fermi energy, which corresponds to $E = 0$ eV in Fig. 2. This energy range is marked in both subplots by a gray zone. In this range, electron energy levels (channels) in the zigzag part have no corresponding channels in the armchair part. As a result, electron transport, around the Fermi energy, from the zigzag to the armchair part of the L-shaped nanoribbon decelerates, because of energy exchange between electrons and the lattice.

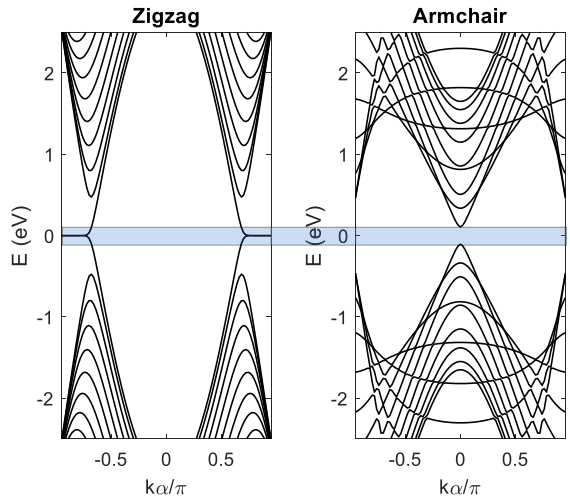

Fig. 2. Graphene energy bands. Left subplot: Energy bands of the zigzag part of the L-shaped nanoribbon (AB and CD). Right subplot: Energy bands of the armchair part of the L-shaped nanoribbon (BF and DE). There are no common electron channels in energy range around E = 0, indicated by the gray zone.

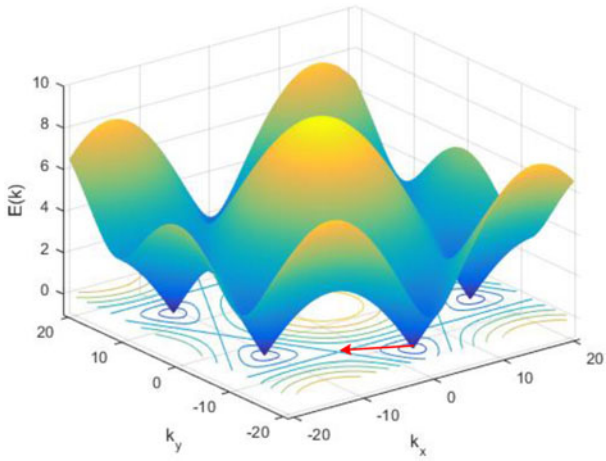

Fig. 3. Graphene conduction band. The (red) arrow indicates the change in electron momentum during transport from the zigzag part (initial point) to the armchair part (end point) of the L-shaped nanoribbon.

In addition to energy exchange between electrons and the graphene lattice described above, electrons are also subjected to scattering during their transport from the zigzag to the armchair part of the graphene nanoribbon. This scattering is depicted in Fig. 3, which shows the graphene conduction band. The dispersion relation for graphene is given by:

$$E(k) = \pm\tau\sqrt{1 + 4\cos\frac{\sqrt{3}\,a\,k_y}{2}\,\cos\frac{a\,k_x}{2} + 4\cos^2\frac{a\,k_x}{2}} \qquad (2)$$

where k_x and k_y are the momentum vector components and a is the distance between two neighboring carbon atoms.

The momentum of electrons transported along the zigzag part is located near the Dirac points and the momentum of electrons transported along the armchair part is located between Dirac points. When the electron transport direction changes by 90°, from the zigzag to the armchair part, there are subjected to scattering indicated by the (red) arrow in Fig. 3. The initial point of the arrow is at a Dirac point and the end point between Dirac points.

The two effects described in this section, when combined, give rise to a pseudo-bandgap, which, as will be shown in the subsequent sections, manifests itself as an electron energy region with zero conductance. This pseudo-bandgap can be further manipulated with the action of top-gate potentials and L-shaped graphene geometries and can serve as a basis for the design of graphene logic gates.

III. Computation Method

The conductance of the graphene logic gates for various input and top-gate potentials will be computed using tight-binding Hamiltonians, as the one of equation (1) and the non-equilibrium Green's function (NEGF) method [14], [15]. In this section we present briefly the computation method and compute, as a reference, the conductance of a rectangular graphene nanoribbon and the conductance of an L-shaped nanoribbon.

In the NEGF method both the retarded Green's function, G^R and the advanced Green's function, G^A, which are actually electron propagators, are used. The retarded Green's function, G^R, is computed from:

$$G^R = [(E + i\eta)I - H - \Sigma_1 - \Sigma_2 - \Sigma_3 - \Sigma_4]^{-1} \quad (3)$$

E is the electron energy, η is a very small positive quantity that ensures the forward electron motion and provides non-zero density of states at the Dirac points [13]–[15]. *I* is the identity matrix, and Σ_1, Σ_2, Σ_3 and Σ_4 are the self-energies of the contacts used in AND, and OR gates. In the case of the NOT gate Σ_4 is set to zero. The advanced Green's function is:

$$G^A = \left(G^R\right)^+ \quad (4)$$

The contact energy broadening factors, Γ_1, Γ_2, Γ_3 and Γ_4 are given by:

$$\Gamma_{1,2,3,4} = i\left[\Sigma_{1,2,3,4} - \Sigma^+_{1,2,3,4}\right] \quad (5)$$

In the case of the NOT gate Γ_4 is zero. The electron density of states is given by:

$$A = i\ \left(G^R - G^A\right) \quad (6)$$

Finally, the conductance as a function of electron energy, between any two of the contacts *i* and *j* of the AND, OR and NOT gates is:

$$G_{i,j}(E) = \frac{2\,q^2}{h} Trace\left[\Gamma_i\ G^R\ \Gamma_j\ G^A\right] \quad (7)$$

where in the case of the AND and OR gates, *i* and *j* take on values 1, 2, 3 or 4 and in the case of the NOT gate 1, 2 and 3.

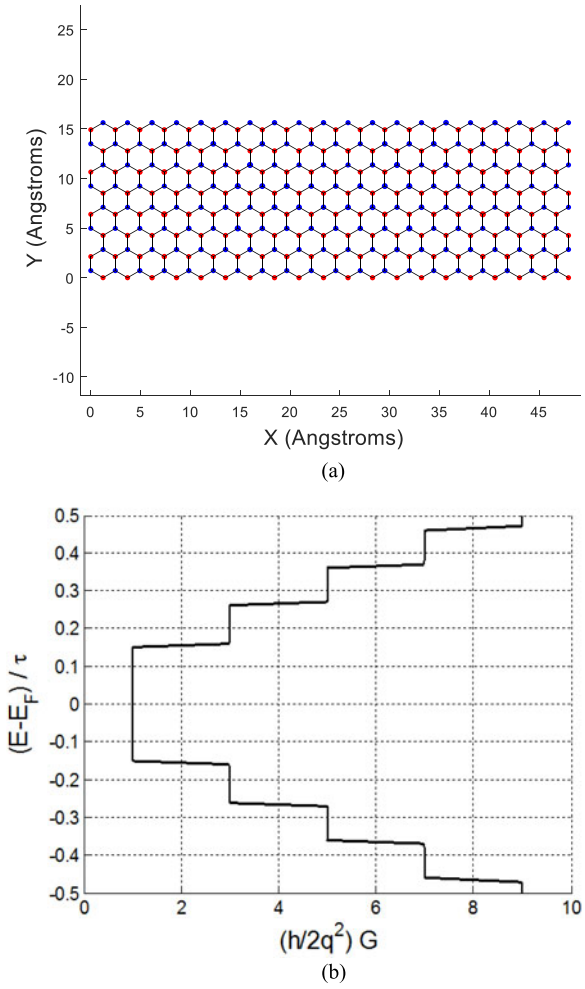

Fig. 4. (a) A rectangular graphene nanoribbon with zigzag edges. (b) The conductance of this nanoribbon computed using the NEGF method.

Fig. 4. shows the conductance of a rectangular graphene nanoribbon with zigzag edges, computed using the NEGF method.

We computed the conductance of the L-shaped nanoribbon shown in Fig. 1, using the NEGF method. The conductance of this nanoribbon as a function of energy is shown in Fig. 5. The pseudo-bandgap appears in this figure as a zero conductance region for energies about ±0.6 arround zero in the $[E - E_F/\tau]$ axis, i.e., ±0.22 eV. This bandgap can be further broadened and its location in the energy axis can be displaced up or down by the action of top gate potentials and the graphene gates geometry, as will be described in the subsequent sections.

IV. The AND Graphene Logic Gate

Fig. 6 shows the graphene AND gate. The top view of the gate is shown in the upper part of the figure and the cross section along the (red) AB line in the lower part.

The gate structure comprises three parallel branches of zigzag edged nanoribbons that merge in an armchair edged nanoribbon. The graphene structure is placed on a substrate, which can be a non-conducting bio-material or an insulating material. Only two

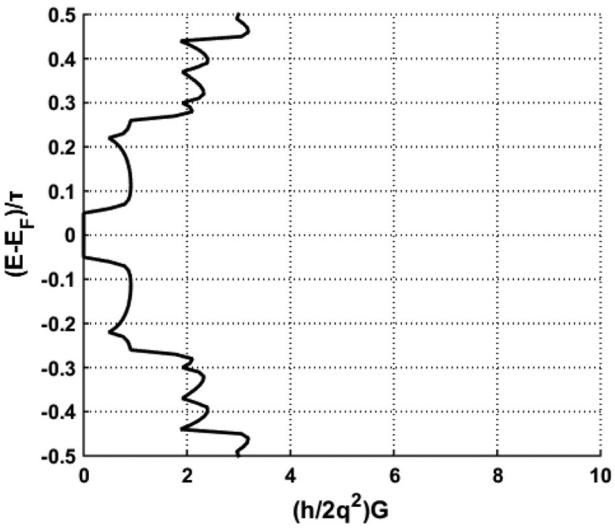

Fig. 5. The conductance of the L-shaped nanoribbon of Fig. 1, computed using the NEGF method.

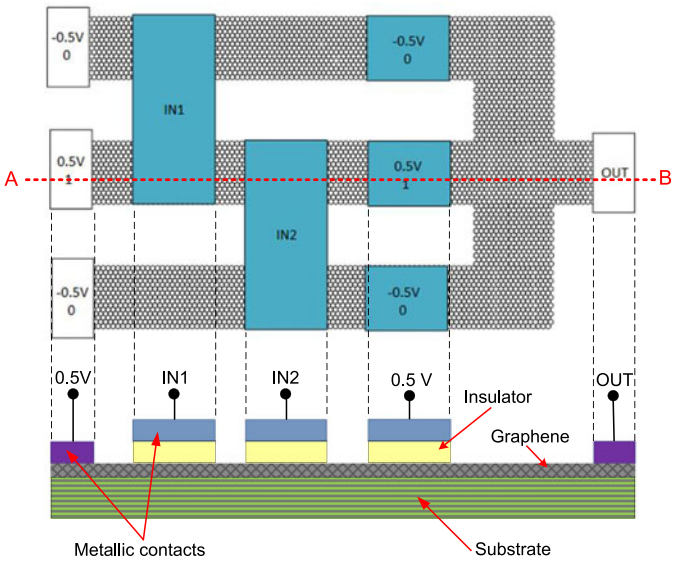

Fig. 6. Up: Top view of the graphene AND gate. Down: Cross section of the graphene AND gate along the (red) AB line.

potential values are used to bias and operate the gate, namely 0.5 V corresponding to logical "1" and −0.5 V corresponding to logical "0". The three, parallel zigzag edged nanoribbon branches are biased with potentials −0.5 V, 0.5 V and −0.5 V, from top to bottom. These potentials are applied through three metallic contacts, which are in direct contact with the graphene layer and remain constant during the gate operation and hereafter will be called biasing contacts. These contacts are represented by white rectangles on the left of the gate, as shown in the upper part of Fig. 6. The up and bottom nanoribbon branches change their edge orientation by 90°, i.e., from zigzag to armchair, whereas the nanoribbon in the middle does not. The armchair edged nanoribbon is connected to the output, OUT, through a direct metallic contact placed on the graphene layer. The three branches are also biased by three top gate potentials with values −0.5 V, 0.5 V and −0.5 V, from top to bottom. These potentials are applied through an insulating layer and remain constant during the operation of the gate.

TABLE I
AND GATE TRUTH TABLE

IN1	IN2	OUT
0, (-0.5 V)	0, (-0.5 V)	0, (-0.5 V)
0, (-0.5 V)	1, (+0.5 V)	0, (-0.5 V)
1, (+0.5 V)	0, (-0.5 V)	0, (-0.5 V)
1, (+0.5 V)	1, (+0.5 V)	1, (+0.5 V)

The two inputs to the gate, IN1 and IN2, are applied through top gates. The input IN1 is applied simultaneously to the top and middle branches, through a common top gate, and the input IN2 is applied simultaneously to the middle and bottom branches, also by a common top gate, as shown in the upper part of Fig. 6. Electron transport from the three biasing contacts to the output contact, OUT, is controlled by the input top gates, IN1 and IN2. If we are to draw an analogy between the graphene and the CMOS AND gates, the potentials with value −0.5 V, which are constantly applied to the up and down biasing contacts, correspond to the CMOS Vss potential, and the potential with value 0.5 V, which is constantly applied to the middle biasing contact, corresponds to the CMOS Vdd potential. The inputs IN1 and IN2 determine which of the two potentials will be transferred to the output, in analogy with the inputs of the CMOS AND gate, which are applied to the gates of the MOSFETs.

Table I shows the truth table of the graphene AND gate. More specifically, it shows the logic values 0 and 1 and the corresponding potentials in the parentheses. Fig. 7 shows the operation of the gate.

Fig. 7 shows the conductance of the three branches of the AND gate. Each of the four Figures, 7(a), 7(b), 7(c) and 7(d) corresponds to one line of the AND gate truth table. The vertical axis represents $(E - E_F)/\tau$ and the Fermi energy is located at $(E - E_F)/\tau = 0$. Only electrons with energies a few kT below and above the Fermi energy participate in the conductance and this energy range is indicated by the yellow bands in Fig. 7.

Fig. 7(a) corresponds to the first line of the truth table, i.e., the case where IN1 $= 0(-0.5\,\text{V})$ and IN2 $= 0(-0.5\,\text{V})$. The conductance of the top branch of the graphene AND gate is shown on the left, the conductance of the middle branch in the middle and the conductance of the bottom branch on the right. The conductance of the middle branch in the energy range of interest is zero and therefore the biasing potential 0.5 V does not reach the gate output. The conductance of the top and bottom branches is nonzero in the energy range of interest, and the biasing potential −0.5 V is transferred to the output, which is set to the logic value 0.

Fig. 7(b) corresponds to the second line of the truth table, where IN1 $= 0(-0.5\,\text{V})$ and IN2 $= 1(+0.5\,\text{V})$. The conductance of the middle and bottom branches in the energy range of interest is zero, whereas the conductance of the top branch is

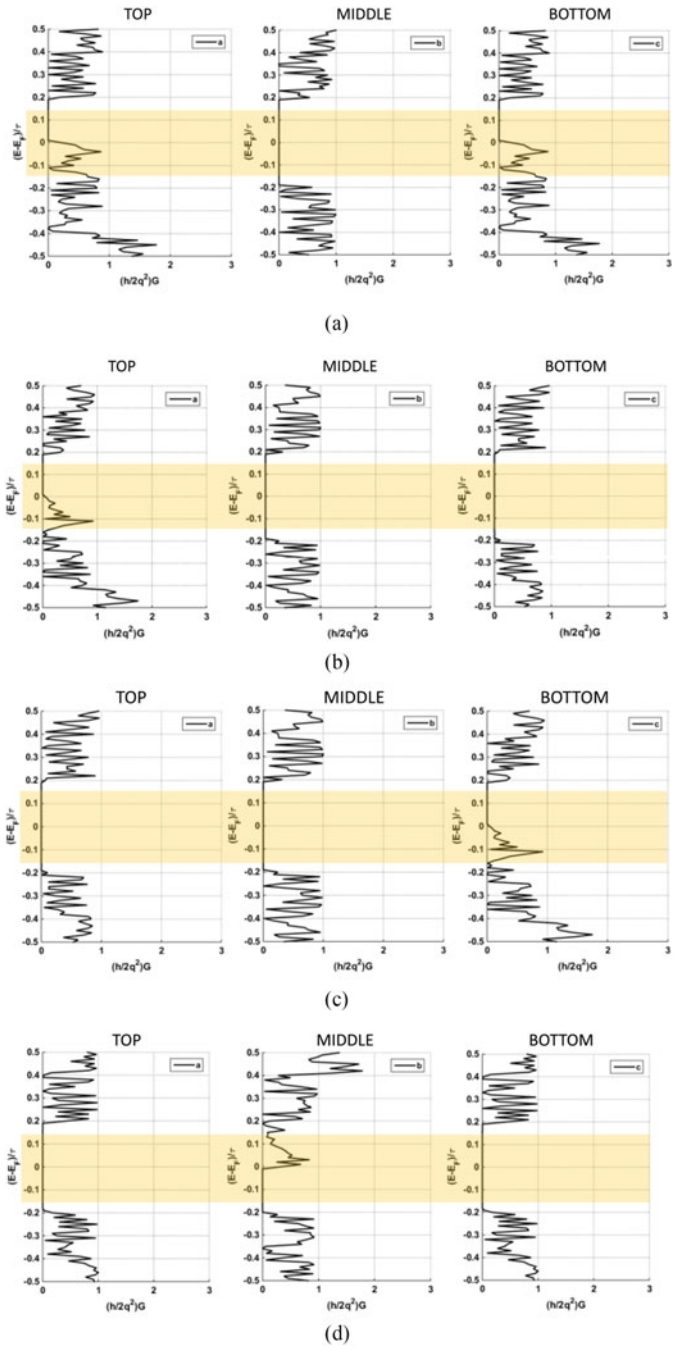

Fig. 7. Conductance of the three graphene AND gate branches. The conductance of the top branch is shown on the left, the conductance of the middle branch, in the middle and the conductance of the bottom branch on the right. Each of the figures (a), (b), (c) and (d) correspond to one line of the gate truth table. The energy range of electrons that participate in the conductance is indicated by yellow bands.

nonzero and the biasing potential -0.5 V is transferred via this branch to the output, which is set to the logic value 0.

Fig. 7(c) corresponds to the third line of the truth table, where IN1 $= 1(+0.5\,\text{V})$ and IN2 $= 0(-0.5\,\text{V})$. The conductance of the top and middle branches in the energy range of interest is zero, whereas the conductance of the bottom branch is nonzero and the biasing potential -0.5 V is transferred via this branch to the output, which is set to the logic value 0.

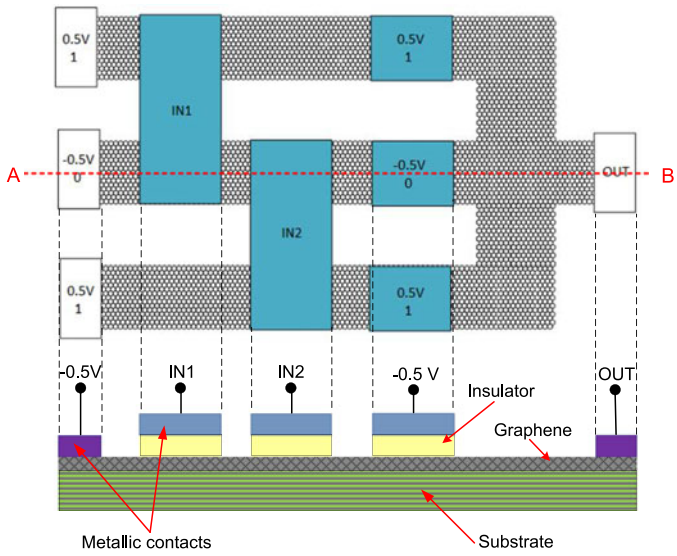

Fig. 8. Up: Top view of the graphene OR gate. Down: Cross section of the graphene OR gate along the (red) AB line.

Fig. 7(d) corresponds to the fourth line of the truth table, where IN1 $= 1(+0.5\,\text{V})$ and IN2 $= 1(+0.5\,\text{V})$. The conductance of the top and bottom branches in the energy range of interest is zero, whereas the conductance of the middle branch is nonzero and the biasing potential $+0.5$ V is transferred via this branch to the output, which is set to the logic value 1.

Therefore, the AND gate truth table is reproduced by the operation of the graphene AND gate, shown in Fig. 6.

V. The OR Graphene Logic Gate

Fig. 8 shows the graphene OR gate. The top view of the gate is shown in the upper part of the figure and the cross section along the (red) AB line at the lower part.

The OR gate structure is the same as the structure of the AND gate. It comprises three parallel branches of zigzag edged nanoribbons that merge in an armchair edged nanoribbon and is placed on a substrate, which can be a non-conducting biomaterial or an insulating material. As in the case of the AND gate, only two potentials are used to bias and operate the gate, 0.5 V and -0.5 V, corresponding to logical "1" and to logical "0". These two potentials in the OR and AND gates are applied at different electrodes. In the OR gate, the biasing potentials at the three, parallel zigzag edged nanoribbon branches are 0.5 V, -0.5 V and 0.5 V, from top to bottom. They are applied through three metallic contacts, which are in direct contact with the graphene layer and remain constant during the gate operation.

In the case of the OR gate the three branches are also biased by three top gate potentials with values 0.5 V, -0.5 V and 0.5 V, from top to bottom. These potentials are applied through an insulating layer and remain constant during the operation of the gate.

The two inputs to the OR gate, IN1 and IN2, are applied through top gates. As in the case of the AND gate, the input IN1 is applied simultaneously to the top and middle branches, through a common top gate, and the input IN2 is applied

TABLE II
OR GATE TRUTH TABLE

IN1	IN2	OUT
0, (-0.5 V)	0, (-0.5 V)	0, (-0.5 V)
0, (-0.5 V)	1, (+0.5 V)	1, (+0.5 V)
1, (+0.5 V)	0, (-0.5 V)	1, (+0.5 V)
1, (+0.5 V)	1, (+0.5 V)	1, (+0.5 V)

simultaneously to the middle and bottom branches, also by a common top gate, as shown in the upper part of Fig. 8. Input top gates IN1 and IN2 control the electron transport from the biasing contacts to the output, OUT. The inputs IN1 and IN2 determine which of the biasing potentials will be transferred to the output.

Table II shows the truth table of the graphene OR gate, and Fig. 9 shows the operation of the gate.

Fig. 9(a) corresponds to the first line of the OR truth table, i.e., the case where IN1 $= 0(-0.5\,\mathrm{V})$ and IN2 $= 0(-0.5\,\mathrm{V})$. The conductance of the top branch of the graphene OR gate is shown on the left, the conductance of the middle branch in the middle and the conductance of the bottom branch on the right. The conductance of the top and bottom branches is zero in the energy range of interest, and the biasing potentials of the top and bottom branches, i.e., $+0.5$ V are not transferred to the output. On the other hand, the conductance of the middle branch in the energy range of interest is nonzero and therefore the biasing potential -0.5 V is transferred to the output, which is set to the logic value 0.

Fig. 9(b) corresponds to the second line of the truth table, where IN1 $= 0(-0.5\,\mathrm{V})$ and IN2 $= 1(+0.5\,\mathrm{V})$. The conductance of the top and middle branches in the energy range of interest is zero, whereas the conductance of the bottom branch is nonzero and the biasing potential $+0.5$ V is transferred via this branch to the output, which is set to the logic value 1.

Fig. 9(c) corresponds to the third line of the truth table, where IN1 $= 1(+0.5\,\mathrm{V})$ and IN2 $= 0(-0.5\,\mathrm{V})$. The conductance of the middle and bottom branches in the energy range of interest is zero, whereas the conductance of the top branch is nonzero and the biasing potential $+0.5$ V is transferred via this branch to the output, which is set to the logic value 1.

Fig. 9(d) corresponds to the fourth line of the truth table of the OR gate, where IN1 $= 1(+0.5\,\mathrm{V})$ and IN2 $= 1(+0.5\,\mathrm{V})$. The conductance of the middle branch in the energy range of interest is zero, whereas the conductance of the top and bottom branches is nonzero and the biasing potentials $+0.5$ V are transferred via these branches to the output, which is set to the logic value 1.

Therefore, the OR gate truth table is reproduced by the operation of the graphene OR gate, shown in Fig. 8.

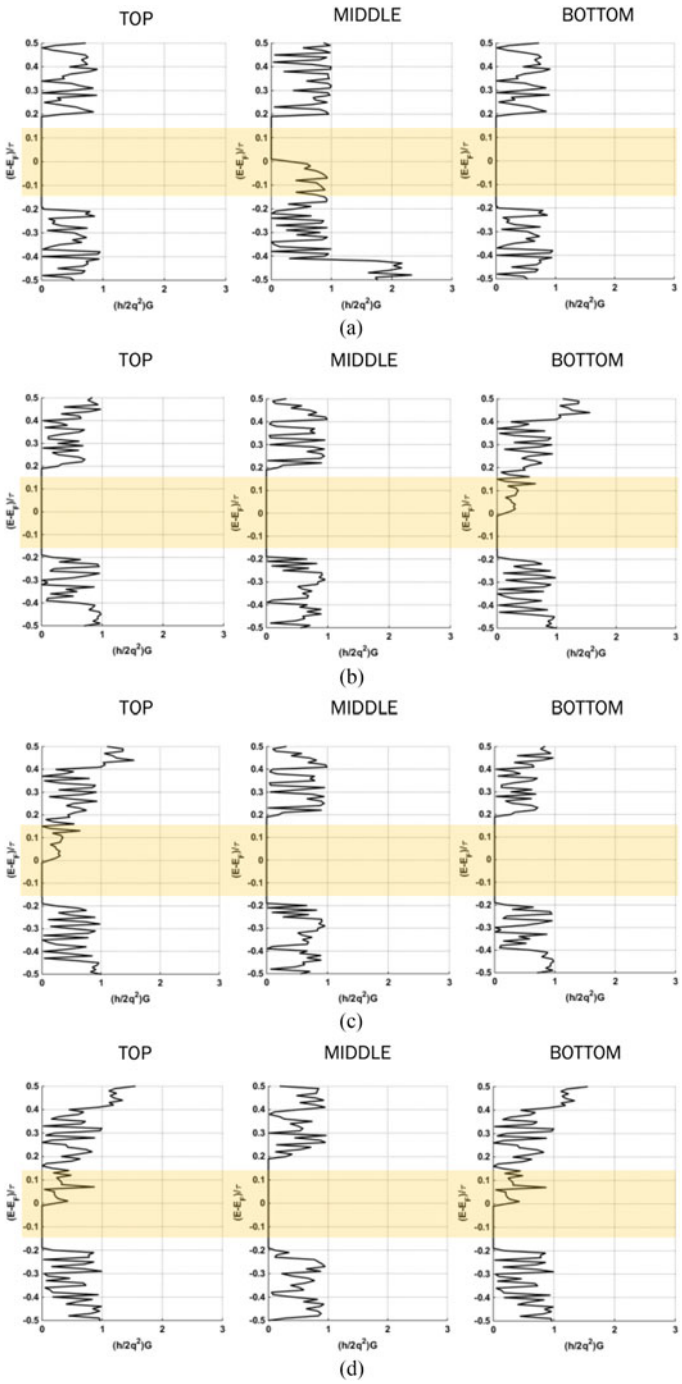

Fig. 9. Conductance of the three graphene OR gate branches. The conductance of the top branch is shown on the left, the conductance of the middle branch, in the middle and the conductance of the bottom branch on the right. Each of the figures (a), (b), (c) and (d) correspond to one line of the gate truth table. The energy range of electrons that participate in the conductance is indicated by yellow bands.

VI. THE NOT GRAPHENE LOGIC GATE

Fig. 10 shows the graphene NOT gate. The top view of the gate is shown in the upper part of the figure and the cross section along the (red) AB line at the lower part.

The NOT gate structure is similar to the structure of the AND, and the OR graphene gates. It comprises only two parallel branches of zigzag edged nanoribbons that both merge in an armchair edged nanoribbon and is also placed on a substrate, which can be a non-conducting bio-material or an insulating material. As in the case of the AND, and OR gates, only two potentials are used to bias and operate the gate, namely,

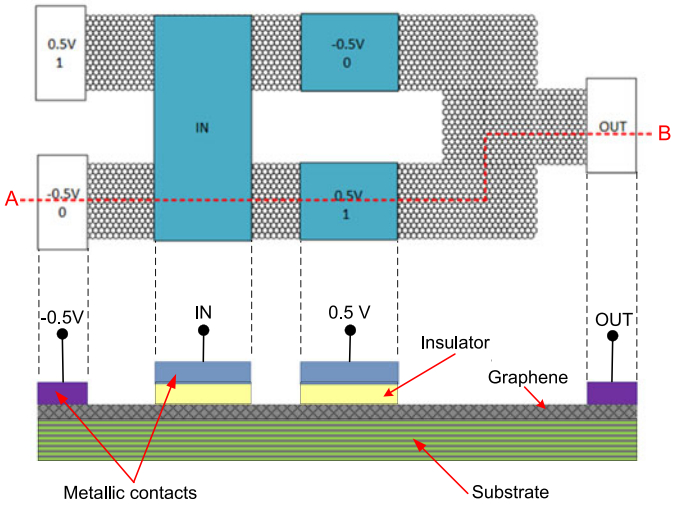

Fig. 10. Up: Top view of the graphene NOT gate. Down: Cross section of the graphene NOT gate along the (red) AB line.

TABLE III
NOT GATE TRUTH TABLE

IN	OUT
0, (-0.5 V)	1, (+0.5 V)
1, (+0.5 V)	0, (-0.5 V)

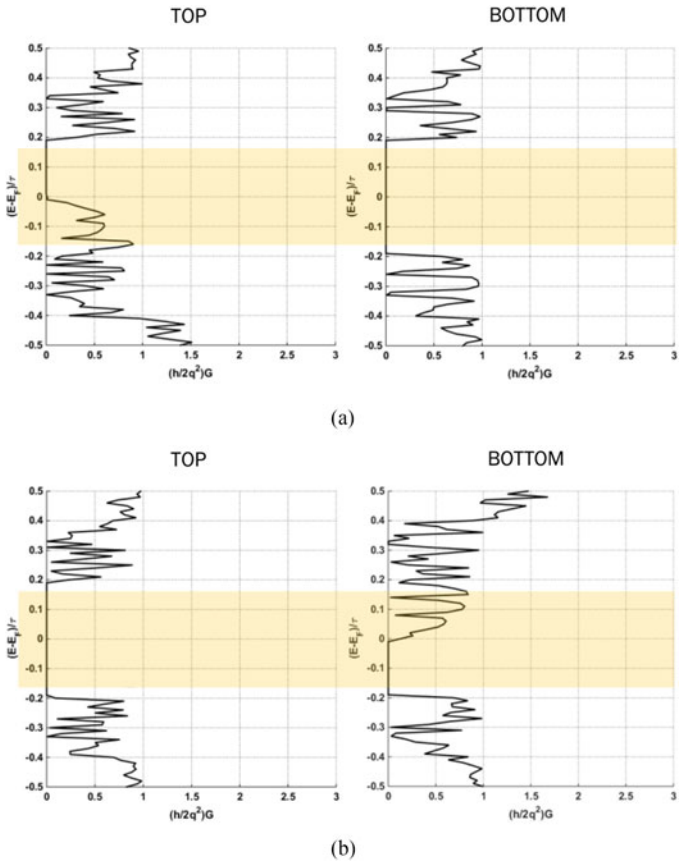

Fig. 11. Conductance of the two graphene NOT gate branches. The conductance of the top branch is shown on the left, and the conductance of the bottom branch on the right. Each of the figures (a) and (b), correspond to one line of the gate truth table. The energy range of electrons that participate in the conductance is indicated by yellow bands.

0.5 V and -0.5 V, corresponding to logical "1" and to logical "0". The biasing potential 0.5 V is applied to the top zigzag edged nanoribbon branch and the biasing potential of -0.5 V is applied to the bottom branch. Both biasing potentials are applied through two metallic contacts, which are in direct contact with the graphene layer, and remain constant during the gate operation.

The two branches of the NOT gate are also biased by two top gate potentials. The top branch top gate potential is -0.5 V and the bottom branch top gate potential is 0.5 V. Both these potentials are applied through an insulating layer and remain constant during the operation of the gate.

The input to the NOT gate, IN, is applied simultaneously to both branches, through a common top gate. The input IN determines which of the biasing potentials will be transferred to the output, OUT.

Table III shows the truth table of the graphene NOT gate, and Fig. 11 shows the operation of the gate.

Fig. 11(a) corresponds to the first line of the NOT truth table, i.e., the case where IN $= 0(-0.5\,\text{V})$. The conductance of the top branch of the graphene NOT gate is shown on the left, and the conductance of the bottom branch on the right. The conductance of the bottom branch is zero in the energy range of interest, and the biasing potential of the bottom branch, i.e., -0.5 V is not transferred to the output. The conductance of the top branch in the energy range of interest is nonzero and therefore the biasing potential of the top branch, $+0.5$ V is transferred to the output, which is set to the logic value 1.

Fig. 11(b) corresponds to the second line of the NOT truth table, i.e., the case where IN $= 1(+0.5\,\text{V})$. Again, the conductance of the top branch of the graphene NOT gate is shown on the left, and the conductance of the bottom branch on the right. The conductance of the top branch is zero in the energy range of interest, and the biasing potential of the top branch, i.e., $+0.5$ V is not transferred to the output. The conductance of the bottom branch in the energy range of interest is nonzero and, therefore the biasing potential of the bottom branch, -0.5 V is transferred to the output, which is set to the logic value 0. We have shown that the NOT gate truth table is reproduced by the operation of the graphene NOT gate, shown in Fig. 10.

VII. CONCLUSION

We designed the three most important logic gates using L-shaped graphene nanoribbons as building blocks and simulated their operation using tight-binding Hamiltonians and the NEGF method. We gave a physical explanation of the feasibility of designing and fabricating graphene logic gates that use L-shaped graphene nanoribbons in Section II. All three graphene gates use two potential values, namely -0.5 V and $+0.5$ V, that correspond to the logic 0 and 1. Our designs are analogous to the designs of the CMOS logic gates. The potentials with value

−0.5 V, which are constantly applied to the biasing contacts, correspond to the CMOS Vss potential, and the potentials with value 0.5 V, which are constantly applied the biasing contacts, corresponds to the CMOS Vdd potential. The gate inputs take on values −0.5 V and +0.5 V and determine which of the biasing potentials will be transferred to the output. Although the graphene gates presented here are to be used in bioelectronic applications, the analogy with CMOS gates allows for the design and fabrication of hybrid graphene/CMOS circuits, in which the graphene circuits will be incorporated into the tissue and can be connected to the CMOS circuitry, that can be placed away from the tissue. Furthermore, the structure of all three graphene gates is similar, because it comprises three or two parallel zigzag edged branches that merge into an armchair branch. This modularity will greatly facilitate the fabrication of graphene logic gates and logic circuits, since, as is well known, any digital circuit can be designed using these gates. By determining the proper modular structure for graphene logic gates, we reduced significantly the parameter space for their fabrication and development, which is the aim of our future work.

REFERENCES

[1] R. Liu *et al.*, "High density individually addressable nanowire arrays record intracellular activity from primary rodent and human stem cell derived neurons," *Nano Lett.*, vol. 17, pp. 2757–2764, 2017.

[2] W. Kim, J. K. Ng, M. E. Kunitake, B. R. Conklin, and P. Yang, "Interfacing silicon nanowires with mammalian cells," *J. Amer. Chem. Soc.*, vol. 129, pp. 7228–7229, 2007.

[3] B. M. Blaschke *et al.*, "Mapping brain activity with flexible graphene micro-transistors," *2D Mater.*, vol. 4, 2017, Art. no. 025040.

[4] S. Syama and P. V. Mohanan, "Safety and biocompatibility of graphene: A new generation nanomaterial for biomedical application," *Int. J. Biol. Macromol.*, vol. 86, pp. 546–555, 2016.

[5] A. H. Castro Neto, F. Guinea, N. M. R. Peres, K. S. Novoselov, and A. K. Geim, "The electronic properties of graphene," *Rev. Modern Phys.*, vol. 81, pp. 109–162, 2009.

[6] E. L. Wolf, *Graphene*. Oxford, U.K.: Oxford Univ. Press, 2014.

[7] A. Fabbro *et al.*, "Graphene-based interfaces do not alter target nerve cells," *ACS Nano.*, vol. 10, pp. 615–623, 2016.

[8] X. Wu, S. J. Ding, K. Lin, and J. Su, "A review on the biocompatibility and potential applications of graphene in inducing cell differentiation and tissue regeneration," *J. Mater. Chem. B*, vol. 5, pp. 3084–3102, 2017.

[9] I. Willner and E. Katz, *Bioelectronics: From Theory to Applications*. Weinheim, Germany: Wiley, 2005.

[10] C. Karunakaran, K. Bhargava, and R. Benjamin, *Biosensors and Bioelectronics*. Amsterdam, Netherlands: Elsevier, 2015.

[11] I. G. Karafyllidis, "Current switching in graphene quantum point contacts," *IEEE Trans. Nanotechnol.*, vol. 13, no. 4, pp. 820–814, Jul. 2014.

[12] H.-Y. Chiu, V. Perebeinos, Y.-M. Lin, and P. Avouris, "Controllable p-n junction formation in monolayer graphene using electrostatic substrate engineering," *Nano Lett.*, vol. 10, pp. 4634–4639, 2010.

[13] C. Bena and G. Montambaux, "Remarks on the tight-binding model of graphene," *New J. Phys.*, vol. 11, 2009, Art. no. 095003.

[14] S. Reich, J. Maultzsch, C. Thomsen, and P. Odrejón, "Tight-binding description of graphene," *Phys. Rev. B*, vol. 66, 2002, Art. no. 035412.

[15] S. Datta, "Nanoscale device modeling: The Green's function method," *Superlattices Microstruct.*, vol. 28, pp. 253–278, 2000.

Savvas Moysidis received the Dipl. Eng. degree in electrical and computer engineering from the Democritus University of Thrace, Komotini, Greece, in 2016. He is currently working toward the Ph.D. degree.

Ioannis G. Karafyllidis received the Dipl. Eng. and Ph.D. degrees in electrical engineering from the Aristotle University of Thessaloniki, Thessaloniki, Greece. In 1992, he joined the Department of Electrical and Computer Engineering, Democritus University of Thrace, Komotini, Greece, as a faculty member, where he is currently a Professor.

Panagiotis Dimitrakis (S'91–M'98–SM'15) received the B.S. and M.S. degrees in physics from the University of Athens, Zografou, Greece, in 1995 and 1998, respectively, and the Ph.D. degree from the National Technical University of Athens, Athens, Greece, in 2006. He is the author of more than 60 papers in peer review journals in the field of semiconductor devices, nonvolatile memories, and organic electronics. He joined NCSR "Demokritos" in 2007, where he is currently a Senior Researcher with the Institute of Nanoscience and Nanotechnology, Athens, Greece.